An efficient GDQ model for vibration analysis of a multiwall carbon nanotube on Pasternak foundation with general boundary conditions

P Soltani, P Bahar and A Farshidianfar

Proceedings of the Institution of Mechanical Engineers, Part C: Journal of Mechanical Engineering Science 2011 225: 1730 originally published online 11 May 2011
DOI: 10.1177/0954406211402555

An efficient GDQ model for vibration analysis of a multiwall carbon nanotube on Pasternak foundation with general boundary conditions

P Soltani[1]*, **P Bahar**[1], and **A Farshidianfar**[2]
[1]Department of Mechanical Engineering, Islamic Azad University-Semnan Branch, Semnan, Iran
[2]Department of Mechanical Engineering, Ferdowsi University of Mashhad, Mashhad, Iran

The manuscript was received on 6 June 2010 and was accepted after revision for publication on 11 February 2011.

DOI: 10.1177/0954406211402555

Abstract: In this article, the free transverse vibrational behaviour of a multiwall carbon nanotube (MWNT) surrounded by a Pasternak-type elastic medium has been determined using a very generalized model. The model has been made on the basis of Timoshenko elastic beam theory which allows the effects of shear deformation and rotary inertia and supports non-coaxial vibration of the adjacent layers of MWNT using interlayer van der Waals forces. The boundary conditions used in this simulation are such that not only standard and conventional kinds, but also all possible forms, of end conditions are applicable. A generalized differential quadrature method is utilized to solve the governing equations with assorted aspect ratios, various boundary conditions, and different foundation stiffnesses. This study shows that the resonant frequencies of MWNTs are strongly dependent on the stiffness of the elastic medium, aspect ratios, and number of walls in carbon nanotubes and, for short nanotubes, the boundary stiffness plays a significant role on the natural frequencies.

Keywords: vibration, generalized differential quadrature method, multiwall carbon nanotubes, Timoshenko beam, Pasternak-type elastic foundation

1 INTRODUCTION

Superior and exceptional electronic, mechanical, and other physical and chemical properties of carbon nanotubes (CNTs), discovered in 1991 [**1**], have transformed them to ideal building blocks for several nano-electro mechanical systems (NEMS) such as oscillators, charge detectors, clocks, field emission devices, and sensors [**2**–**9**]. Since these devices work mostly with the basis of an oscillating nanotube, vibrational characteristics, and modelling of CNTs have been of great interest in nano-engineering.

*Corresponding author: Department of Mechanical Engineering, Islamic Azad University-Semnan Branch, Semnan, Iran.
emails: p.soltani@semnaniau.ac.ir; payam.soltani@gmail.com; soltanip2@asme.org

Moreover, experiments at the nanoscale are still extremely difficult and molecular dynamics (MD) simulations remain expensive and formidable for large-scale systems. Continuum mechanics models have been effectively and successfully used to simulate the mechanical behaviour of CNTs such as bending, buckling and vibrating [**10**–**14**]. Euler–Bernoulli beam theory is widely used for modelling nanotubes and in some previous works, multiwall carbon nanotubes (MWNTs) have been modelled as a single-Euler-elastic-beam, disregarding non-coaxial intertube radial displacements [**15**, **16**]. Both rotary inertia (RI) and shear deformation (SD) are taken into account by Timoshenko beam theory which simulates vibrational characteristics of nanotubes with more accuracy, especially for stubby CNTs [**17**–**19**].

The van der Waals (vdW) forces between layers in MWNTs play an important role in the movement of nested tubes and directly affect natural frequencies and mode shapes. Hence, to apply a more accurate simulation, several papers used multiple elastic beams to model the effects of the interlayer vdW forces [**19**–**21**].

Furthermore, CNTs are usually surrounded by other materials such as polymers in nanocomposites and the effects of these media should be included in vibrational simulations. Typically, a Winkler-type elastic foundation is employed to model an elastic medium around nanotubes [**19**, **21**–**25**]. The Winkler model is approximated as a series of closely spaced, mutually independent, vertical linear elastic springs and the foundation modulus is represented by stiffness of the springs. A Pasternak-type foundation model, meanwhile, describes a more clarified simulation for an elastic medium using a shear layer with linear elastic springs and therefore, the two different constants express the stiffness of the medium. As a result, some papers applied the Pasternak model for the foundation of nano-materials and nanotubes successfully [**26**–**30**].

In all the mentioned papers, typical boundary conditions such as pinned–pinned (PP), clamped–pinned (CP), free–free (FF), clamped–free (CF), and clamped–clamped (CC) conditions have been employed to investigate the effects of end conditions on the vibrational behaviour of CNTs. Furthermore, some recent studies reveal that the heterogeneous boundary conditions affect the structural stiffness, natural frequency, and buckling behaviours of MWNTs [**31**, **32**]. However, in real applications like nanocomposites, it is particularly hard to predict the accurate boundary stiffness of a CNT embedded in a matrix, and the end constraint may vary from the free condition to clamped condition.

In this study, for the first time, we develop a very general simulation for transverse vibration of MWNTs using the Timoshenko elastic beam model. Our model covers the effects of vdW forces and non-coaxial vibration of internal layers, has no limitation for the number of walls, and supports a Pasternak-type foundation model. Moreover, applying a non-classical form of boundary conditions has made this model more coincident with real situations in NEMS and nanocomposites. The governing equations have been solved numerically for natural frequencies and corresponding mode shapes, using the generalized differential quadrature method (GDQM). The GDQM is a rather efficient and alternative discrete approach for solving the equilibrium equations in engineering and mathematics directly [**33**–**41**]. The obtained results have been compared with some previous, simpler studies, which show a very good agreement and verify the simulation.

2 GOVERNING EQUATIONS

Timoshenko beam theory has been used to investigate the free vibration of MWNT. Hence, the deflection $w(x,t)$ and the slope $\varphi(x,t)$ of a Timoshenko beam with Pasternak elastic foundation are determined by the following two coupled equations [**17**–**19**].

$$\rho A\frac{\partial^2 w}{\partial t^2} - KGA\left(\frac{\partial^2 w}{\partial x^2} - \frac{\partial \phi}{\partial x}\right) = k_p\frac{\partial^2 w}{\partial x^2} + k_e w \tag{1a}$$

$$\rho I\frac{\partial^2 \varphi}{\partial t^2} - EI\frac{\partial^2 \varphi}{\partial x^2} - KGA\left(\frac{\partial w}{\partial x} - \varphi\right) = 0 \tag{1b}$$

where x is the axial coordinate, A and I the cross-sectional area and the second moment of area of the cross-section, respectively, and ρ the mass density per unit volume. In addition, the shear correction factor, the Young's modulus, and the shear modulus of the beam are represented by K, E, and G, respectively. Also, k_p and k_e are the shear stiffness and elastic stiffness of the Pasternak-type foundation model, correspondingly.

3 MULTI-TIMOSHENKO BEAM MODEL

A multi-beam model has been developed and applied for the analysis of the free vibration of MWNTs [**14**]. The applied model is based on Timoshenko elastic theory and assumes that all the nested, concentric single-walled CNTs are individually described by an elastic beam. In this way, the effects of transverse SD and RI are considered for each nanotube of the MWNT. The vdW interaction between nested CNTs and the Pasternak-type foundation are employed for modelling of the nanotube. (Fig. 1).

The deflection of the adjacent tubes is coupled through the vdW force, which is determined by the interlayer spacing. By applying equation (1) for a

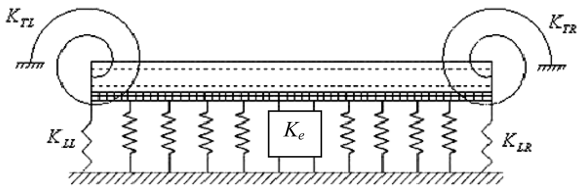

Fig. 1 Model of MWNTs, surrounded by an Pasternak elastic medium with general form of BCs

MWNT with M tubes, the 2-M coupled governing equations are obtained

$$\rho A_1 \frac{\partial^2 w_1}{\partial t^2} - K_1 G A_1 \left(\frac{\partial^2 w_1}{\partial x^2} - \frac{\partial \varphi_1}{\partial x} \right) = c_1 (w_2 - w_1)$$

$$\rho I_1 \frac{\partial^2 \varphi_1}{\partial t^2} - EI_1 \frac{\partial^2 \varphi_1}{\partial x^2} - K_1 G A_1 \left(\frac{\partial w_1}{\partial x} - \varphi_1 \right) = 0$$

$$\rho A_2 \frac{\partial^2 w_2}{\partial t^2} - K_2 G A_2 \left(\frac{\partial^2 w_2}{\partial x^2} - \frac{\partial \varphi_2}{\partial x} \right) = -c_1 (w_2 - w_1) + c_2 (w_3 - w_2) \tag{2a}$$

$$\rho I_2 \frac{\partial^2 \varphi_2}{\partial t^2} - EI_2 \frac{\partial^2 \varphi_2}{\partial x^2} - K_2 G A_2 \left(\frac{\partial w_2}{\partial x} - \varphi_2 \right) = 0 \tag{2b}$$

$$\vdots$$

$$\rho A_M \frac{\partial^2 w_M}{\partial t^2} - K_M G A_M \left(\frac{\partial^2 w_M}{\partial x^2} - \frac{\partial \varphi_M}{\partial x} \right) = k_p \frac{\partial^2 w_M}{\partial x^2} - c_{M-1} (w_M - w_{M-1}) + k_e w_M$$

$$\rho I_M \frac{\partial^2 \varphi_M}{\partial t^2} - EI_M \frac{\partial^2 \varphi_M}{\partial x^2} - K_M G A_M \left(\frac{\partial w_M}{\partial x} - \varphi_M \right) = 0 \tag{2m}$$

where $w_j(x,t)$ and $\varphi_j(x,t)$ $(j = 1, 2, \ldots, M)$ are the total deflection and the slope due to bending of the jth nanotube, t is the time, and I_j and A_j the moment of inertia and the area of the cross-section of the jth tube, in that order. All tubes have the same Young's modulus E and the shear modulus G (with Poisson ratio $\nu = 0.25$). Also, K_j is the shear correction factor of the jth tube while the vdW interaction coefficients c_j are different for each layer and can be determined by equations (3) and (4) [**41**].

$$K_j = \frac{6(1+\nu)(1+\alpha_j)^2}{(7+6\nu)(1+\alpha_j)^2 + (20+12\nu)\alpha_j^2} \tag{3}$$

$$c_j = \frac{320 \times \left(2R_j\right) \frac{erg}{cm^2}}{0.16\Delta^2}, \quad \Delta = 0.142\,\text{nm}, \quad j = 1, 2, \ldots, M-1 \tag{4}$$

where $\alpha_j = (2R_{1j} - th)/(2R_{2j} + th)$ that R_{1j}, R_{2j} are the innermost and outermost radii of jth tube, respectively ($j = 1, 2, \ldots, M$). Also, th is the effective thickness of a single-walled nanotube in which R_j is the average radius of jth tube.

4 GENERAL FORM OF BOUNDARY CONDITIONS

In this model, the general form of boundary conditions (BCs) has been introduced. Applying torsional and linear stiffnesses at the ends of each nanotube has made the model well matched for real conditions and permits it to cover all possible BCs. Thus, BCs for each layer can be expressed as follows:

$$\text{At} \quad x = 0, \begin{cases} K_j G A_j \left(\frac{\partial w_j}{\partial x} - \phi_j \right) = -K_{LL} w_j (0, t). \\ EI_j \frac{\partial \phi_j}{\partial x} = K_{TL} \phi_j (0, t). \end{cases} \tag{5a}$$

$$\text{At} \quad x = l, \begin{cases} K_j G A_j \left(\frac{\partial w_j}{\partial x} - \phi_j \right) = -K_{LR} w_j (l, t). \\ EI_j \frac{\partial \phi_j}{\partial x} = K_{TR} \phi_j (l, t). \end{cases} \tag{5b}$$

$$j = 1, \ldots, M$$

where K_{LL} and K_{TL} denote the linear and the torsional stiffness constants for the left end of nanotube and K_{LR} and K_{TR} the linear and the torsional stiffness constants for the right end. Table 1 introduces several BCs with their relevant values of linear and torsional spring constants.

5 THE GENERALIZED DIFFERENTIAL QUADRATURE METHOD

The Generalized differential quadrature (GDQ) method will be used to discretize the derivatives in the governing equations in terms of displacements and the boundary and compatibility conditions.

The essence of the GDQ method is that the nth order derivative of a smooth one-dimensional function $U(x)$ defined over an interval $[0, L]$ at the ith point of abscissa x_i, can be approximated as

$$\frac{\mathrm{d}^r U(x_i)}{\mathrm{d}x^r} = \sum_{l=1}^{N} C_{il}^{(r)} U(x_i), \quad (i = 1, 2, \ldots, N) \tag{6a}$$

where $C_{il}^{(r)}$ is the weighting coefficient corresponding to the rth order derivative at point x_i and $M' = \sum_{i=1}^{N} n_i$ the number of the total independent variables U_k, which are expressed in series as

$$\{U\}^T = \{U_1, U_2, \ldots, U_k, \ldots, U_{M'}\} = \left\{ w_{j1}^{(0)}, w_{j1}^{(1)}, \varphi_{j1}^{(0)}, \varphi_{j1}^{(1)}, w_{j2}^{(0)}, \varphi_{j2}^{(0)}, \ldots, w_{jN}^{(0)}, w_{jN}^{(1)}, \varphi_{jN}^{(0)}, \varphi_{jN}^{(1)} \right\}$$
$$j = 1, \ldots, M \tag{6b}$$

where $w_{ji}^{(0)}$, $\phi_{ij}^{(0)} = w(x_{ji})$, $\phi(x_{ji}) = w_{ji}$, ϕ_{ji} are the function values.

Table 1 The values of spring constants for several boundary conditions

Boundary conditions	Stiffness (N/m)			
	K_{LL}	K_{TL}	K_{LR}	K_{TR}
PP	∞	0	∞	0
CC	∞	∞	∞	∞
FF	0	0	0	0
CP	∞	∞	∞	0
CF	∞	∞	0	0
Clamped–slide (CS)	∞	∞	0	∞
Pinned–free (PF)	∞	0	0	0

The weighting coefficients for rth-order derivative are given by recurrence relations in general form as

$$C_{il}^{(1)} = \frac{M^{(1)}(x_i)}{(x_i - x_l)M^{(1)}(x_l)}, \quad \text{for} \quad i \neq l, \quad i,\, l = 1,\, 2, \ldots,\, N \tag{6c}$$

$$C_{il}^{(m)} = m\left(C_{ii}^{(m-1)} C_{il}^{(1)} - \frac{C_{il}^{(m-1)}}{x_i - x_l}\right), \quad \text{for} \quad i \neq l,\ m \geq 2 \quad i,\, l = 1, \ldots, N \tag{6d}$$

$$C_{il}^{(m)} = -\sum_{l=1, l\neq i}^{N} C_{il}{}^{(m)}. \quad i = 1,\, 2,\, \ldots,\, N \tag{6e}$$

where

$$M(x_i) = \prod_{l=1}^{N} (x - x_l) \tag{6f}$$

These recurrence expressions are very useful for implementation in computer programming. There is no need to solve a set of algebraic equations to find weighting coefficients and there is no influence of loading or BCs on the weighting coefficients.

Besides the selection of test functions and the derivation of the explicit weighting coefficients, the judicious choice of the sampling points is another important matter in GDQM. We divide the solution domain [0, L] using both equispaced points (equation (6g)) and cosine-type (or Gauss–Chebyshev–Lobatto) points (equation (6h)) as

$$x_i = \frac{i-1}{N-1} \times L \tag{6g}$$

$$x_i = \frac{1}{2}\left[1 - \cos\left(\frac{i-1}{N-1}\pi\right) \times L\right], \quad i = 1,\, 2,\, \ldots,\, N \tag{6h}$$

It has been proven that for the Lagrange interpolating polynomials, the Gauss–Chebyshev–Lobatto sampling points rule guarantees convergence and efficiency to the GDQ technique [**42**–**44**].

6 SOLUTION METHODOLOGY

6.1 Dimensionless parameters

The deflection and the slope of the each wall of the MWNT can be given by

$$w_j = W_j e^{i\omega t},\ \varphi_j = \psi_j e^{i\omega t}. \quad j = 1,\, 2,\, \ldots,\, M \tag{7}$$

where $i = \sqrt{-1}$, ω is the vibrational frequency and W_j and ψ_j the mode shapes for transverse deflection and slope of jth tube. For convenience and generality, the following non-dimensional variables are defined in the present analysis

$$\bar{W}_j = \frac{W_j}{l},\ \xi = \frac{x}{l},\ \mu_j = \frac{\rho A_j l^4}{EI_j},\ \gamma_j = \frac{K_j G A_j l^2}{EI_j} \tag{8a}$$

$$\alpha_j = \frac{A_j l^2}{I_j},\ \beta_j = \frac{K_j G A_j^2 l^4}{EI_j^2},\ k_e^* = \frac{k_e l^4}{EI_M},\ k_p^* = \frac{k_p l^4}{EI_M} \tag{8b}$$

$$\varepsilon_j = \frac{c_s l^4}{EI_j}, \quad \text{for } s = 1,\, 2\,,\, \ldots,\, M-1 \tag{8c}$$

$$\varepsilon_k^* = \frac{c_k l^4}{EI_k}, \quad \text{for } k = 2,\, 3\,,\, \ldots,\, M-1 \tag{8d}$$

and the BCs

$$(K_{LL})_j^* = \frac{(K_{LL})_j l}{K_j G A_j},\ (K_{LR})_j^* = \frac{(K_{LR})_j l}{K_j G A_j} \tag{9a}$$

$$(K_{TL})_j^* = \frac{(K_{TL})_j l}{EI_j},\ (K_{TR})_j^* = \frac{(K_{TR})_j l}{EI_j} \tag{9b}$$

Substituting equations (8), (9) into equations (2), (5) yields dimensionless vibration governing equations of the system

$$-\mu_1\omega^2\bar{W}_1 - \gamma_1\left(\frac{\partial\bar{W}_1}{\partial\xi^2} - \frac{\partial\psi_1}{\partial\xi}\right) = \varepsilon_1(\bar{W}_2 - \bar{W}_1)$$
$$-\mu_1\omega^2\psi_1 - \alpha_1\frac{\partial^2\psi_1}{\partial\xi^2} - \beta_1\left(\frac{\partial\bar{W}_1}{\partial\xi} - \psi_1\right) = 0 \tag{10a}$$

$$-\mu_2\omega^2\bar{W}_2 - \gamma_2\left(\frac{\partial\bar{W}_2}{\partial\xi^2} - \frac{\partial\psi_2}{\partial\xi}\right) = -\varepsilon_2(\bar{W}_2 - \bar{W}_1) + \varepsilon_2^*(\bar{W}_3 - \bar{W}_2)$$
$$-\mu_2\omega^2\psi_2 - \alpha_2\frac{\partial^2\psi_2}{\partial\xi^2} - \beta_2\left(\frac{\partial\bar{W}_2}{\partial\xi} - \psi_2\right) = 0 \tag{10b}$$

$$\vdots$$

$$-\mu_1\omega^2\bar{W}_M - \gamma_M\left(\frac{\partial\bar{W}_M}{\partial\xi^2} - \frac{\partial\psi_M}{\partial\xi}\right) = k_p^*\frac{\partial\bar{W}_M}{\partial\xi^2} - \varepsilon_M(\bar{W}_M - \bar{W}_{M-1}) + k_e^*\bar{W}_M$$
$$-\mu_M\omega^2\psi_M - \alpha_M\frac{\partial^2\psi_M}{\partial\xi^2} - \beta_M\left(\frac{\partial\bar{W}_M}{\partial\xi} - \psi_M\right) = 0 \tag{10m}$$

and the BCs

$$\text{At} \quad \xi = 0, \begin{cases} \frac{\partial\bar{W}_j}{\partial\xi} - \psi_j = (K_{LL})_j^*\bar{W}_j \\ \frac{\partial\psi_j}{\partial\xi} = (K_{TL})_j^*\psi_j \end{cases} \tag{11a}$$

$$\text{At} \quad \xi = 1, \begin{cases} \frac{\partial\bar{W}_j}{\partial\xi} - \psi_j = (K_{LR})_j^*\bar{W}_j \\ \frac{\partial\psi_j}{\partial\xi} = (K_{TR})_j^*\psi_j \end{cases} \tag{11b}$$

6.2 GDQM formulation

By dividing every tube into N segments and applying GDQM to equations (10) and (11), the GDQM formulation for MWNTs with M different nested tubes will be obtained.

$$
\begin{aligned}
&-\mu_1\omega^2\bar{W}_{1i}-\gamma_1\left(\sum_{l=1}^{N}C_{il}^2\bar{W}_{1l}-\sum_{l=1}^{N}C_{il}^1\psi_{1l}\right)\\
&\quad=\varepsilon_1\left(\bar{W}_{2i}-\bar{W}_{1i}\right)\\
&-\mu_1\omega^2\psi_{1i}-\alpha_1\sum_{l=1}^{N}C_{il}^2\psi_{1l}-\beta_1\left(\sum_{l=1}^{N}C_{il}^1\bar{W}_{1l}-\psi_{1i}\right)=0
\end{aligned}
\tag{12a}
$$

$$
\begin{aligned}
&-\mu_2\omega^2\bar{W}_{2i}-\gamma_2\left(\sum_{l=1}^{N}C_{il}^2\bar{W}_{2l}-\sum_{l=1}^{N}C_{il}^1\psi_{2l}\right)=\\
&\qquad-\varepsilon_2\left(\bar{W}_{2i}-\bar{W}_{1i}\right)+\varepsilon_2^*\left(\bar{W}_{3i}-\bar{W}_{2i}\right)\\
&-\mu_2\omega^2\psi_{2i}-\alpha_2\sum_{l=1}^{N}C_{il}^2\psi_{2l}-\beta_2\left(\sum_{l=1}^{N}C_{il}^1\bar{W}_{2l}-\psi_{2i}\right)=0
\end{aligned}
\tag{12b}
$$

$$\vdots$$

$$
\begin{aligned}
&-\mu_M\omega^2\bar{W}_{Mi}-\gamma_M\left(\sum_{l=1}^{N}C_{il}^2\bar{W}_{Ml}-\sum_{l=1}^{N}C_{il}^1\psi_{Ml}\right)=\\
&\quad k_p^*\sum_{l=1}^{N}C_{il}^2\bar{W}_{Ml}-\varepsilon_M\left(\bar{W}_{Mi}-\bar{W}_{(M-1)i}\right)\\
&\qquad+k_e^*\bar{W}_{Mi}-\mu_M\omega^2\psi_{Mi}-\alpha_M\sum_{l=1}^{N}C_{il}^2\psi_{Ml}\\
&\qquad\qquad-\beta_M\left(\sum_{l=1}^{N}C_{il}^1\bar{W}_{Ml}-\psi_{Mi}\right)=0\\
&i=2,\,3,\,\ldots,\,N-1
\end{aligned}
\tag{12m}
$$

with BCs:

$$
\text{At}\quad \xi=0,1\begin{cases}\bar{W}_{ji}^1-\psi_{ji}=Z\bar{W}_{ji}\\ \psi_{ji}^1=S\psi_{ji}\end{cases}
\tag{13}
$$

$$
\begin{aligned}
&i=1\text{ or }N,\quad j=1,\,2,\ldots\,comma\;M,\\
&Z=(K_{LL})_j^*\text{ or }(K_{LR})_j^*,\quad S=(K_{TL})_j^*\text{ or }(K_{TR})_j^*
\end{aligned}
$$

6.3 Eigenvalue equation

By rearranging equations (12) and (13), an assembled form of governing equations with the boundary conditions is given as follows [**36**, **37**]

$$
\begin{bmatrix}[K_{bb}] & [K_{bd}]\\ [K_{db}] & [K_{dd}]\end{bmatrix}\begin{Bmatrix}\{U_b\}\\ \{U_d\}\end{Bmatrix}-\omega^2\begin{bmatrix}[0] & [0]\\ [M_{db}] & [M_{dd}]\end{bmatrix}\begin{Bmatrix}\{U_b\}\\ \{U_d\}\end{Bmatrix}=0
\tag{14a}
$$

where

$$
\{U_b\}=\left\{\bar{W}_{j1},\,\bar{W}_{j1}^1,\,\psi_{j1},\,\psi_{j1}^1,\,\bar{W}_{jM},\,\bar{W}_{jM}^1,\,\psi_{jM},\,\psi_{jM}^1\right\}
\tag{14b}
$$

$$
\{U_d\}=\left\{\bar{W}_{j2},\,\psi_{j2},\,\bar{W}_{j3},\,\psi_{j3},\ldots,\,\bar{W}_{j(M-1)},\,\psi_{j(M-1)}\right\}
\tag{14c}
$$

By matrix subtraction, one has the following generalized eigenvalue equation

$$
([K]-\omega^2[M])\{U_d\}=0
\tag{14d}
$$

where

$$
\begin{aligned}
[K]&=[K_{dd}]-[K_{db}][K_{bb}]^{-1}[K_{bd}],\\
[M]&=[M_{dd}]-[M_{db}][M_{bb}]^{-1}[M_{bd}]
\end{aligned}
$$

To obtain a non-trivial solution for the above equation, it is required that the determinant of the coefficient matrix vanishes

$$
\det\left([K]-\omega^2[M]\right)=0
\tag{14e}
$$

where $[K]$, $[M]$, and ω stand for the stiffness matrix, the mass matrix, and non-dimensional natural frequencies, respectively.

7 NUMERICAL RESULTS AND DISCUSSION

For the numerical calculations, the properties and the dimensions of MWNT are assumed as follows: $E=1$ TPa, $G=0.4$ TPa, and $\rho=2.3\ \frac{\text{g}}{\text{cm}^3}$ and the innermost radius of the inner tube is $r_{\text{in}}=0.35$ nm. Additionally, we consider an average thickness of 0.35 nm for each wall and also a 0.35 nm as an annulus. The length of the tube is selected such that $\frac{L}{d_{\text{ave}}}=10$, 30, 50, and 100.

For verification, the non-dimensional natural frequencies are found using GDQM and given in Tables 2, 3, and 4 for the first three modes, respectively. The results for CC, CF, and PP boundary conditions are compared with the results in references [**19**] and [**41**], respectively. The present model, as a general simulation which supports all kinds of BCs and mediums of a MWNT, shows a good agreement with all the previous studies.

7.1 Natural frequencies

As mentioned before, the natural frequencies and the associated mode shapes of MWNTs are calculated using the GDQM model. In Fig. 2, dimensional natural frequencies ω_n of a clamped-clamped MWNT with various aspect ratios L/d have been shown for a DWNT ($M=2$) and a five-walled MWNT ($M=5$). It is clear that the dimensional natural frequency ω_n increases with the decreasing aspect ratio L/d.

Table 2 The first three non-dimensional natural frequencies of a CC double-walled CNT ($k_p = k_e = 0$) (comparison of results)

Aspect ratio	Mode number, n	Natural frequency	
		Present (GDQM)	Reference [**19**]
$\frac{L}{d} = 10$	1	4.458 5	4.553 3
	2	6.977 2	7.249 3
	3	9.204 3	9.697 8
$\frac{L}{d} = 30$	1	4.695 0	4.708 7
	2	7.722 8	7.771 8
	3	10.685	10.799
$\frac{L}{d} = 50$	1	4.717 2	4.722 2
	2	7.804 7	7.8234
	3	10.877	10.922
$\frac{L}{d} = 100$	1	4.726 8	4.728 0
	2	7.8409	7.845 7
	3	10.965	10.997

Table 3 The first three non-dimensional natural frequencies of CF double-walled CNT ($k_p = k_e = 0$) (comparison of results)

Aspect ratio	Mode number, n	Natural frequency	
		Present (GDQM)	Reference [**19**]
$\frac{L}{d} = 10$	1	1.861 0	1.866 3
	2	4.474 4	4.550 3
	3	7.1092	7.343 7
$\frac{L}{d} = 30$	1	1.873 5	1.874 1
	2	4.666 6	4.676 9
	3	7.747 8	7.787 2
$\frac{L}{d} = 50$	1	1.874 5	1.874 7
	2	4.684 1	4.687 8
	3	7.815 2	7.830 0
$\frac{L}{d} = 100$	1	1.874 9	1.875 0
	2	4.691 5	4.692 5
	3	7.844 7	7.848 5

Furthermore, the slope of the curves, which represents the difference between frequencies in different modes, is steeper for short CNTs with small values of L/d. This means that for stubby CNTs the effects of RI and SD will be more obvious and give rise to the natural frequency ω_n especially for higher vibrational modes.

The effects of the number of walls M on the natural frequencies ω_n, for a short ($L/d = 10$) and a long ($L/d = 100$) CNT, have been demonstrated in Fig. 3. This figure reveals that the number of walls in a CNT affects the dimensional natural frequency ω_n and for a CNT with a greater number of walls M, the natural frequencies are reduced to smaller values. In fact, both the mass of MWNTs and the vdW forces between walls increase with an increase in the number of walls M, but the results indicate that the effects of the vdW forces on the stiffness of the system are not very significant compared with the effects of the mass increasing for large values of M.

Table 4 The first three non-dimensional natural frequencies of PP double-walled CNT ($k_p = k_e = 0$) (comparison of results)

Aspect ratio	Mode number, n	Natural frequency	
		Present (GDQM)	Reference [**39**]
$\frac{L}{d} = 10$	1	3.092 6	3.127 8
	2	5.937 1	6.173 5
	3	8.734 5	9.041 8
$\frac{L}{d} = 30$	1	3.128 9	3.137 5
	2	6.185 3	6.256 1
	3	9.111 9	9.333 1
$\frac{L}{d} = 50$	1	3.139 5	3.141 0
	2	6.266 9	6.278 9
	3	9.370 3	9.410 2
$\frac{L}{d} = 100$	1	3.141 0	3.141 4
	2	6.279 0	6.281 7
	3	9.410 9	9.421 1

Figs 4 and 5 focus on the effects of the elastic medium around a CNT. The dependency of the first natural frequency ω_1 on elastic constant k_e and shear constant k_p of the Pasternak foundation model has been shown for a DWNT ($M = 2$) and a MWNT ($M = 5$) with a CC boundary condition. As seen, by increasing the elastic constant k_e, the natural frequency ω_1 rises markedly especially for low shear constants k_p and small aspect ratio L/d. For a better understanding of this, some helpful numerical results have been given in Table 5.

7.2 General boundary conditions

As mentioned above, BCs of an embedded CNT depend on the bonds between carbon atoms within the medium at each end of nanotube. Hence, it is difficult to predict the real stiffness of the ends of a CNT embedded in a matrix. Furthermore, BCs affect the natural frequencies directly and significantly and it seems that the standard and the traditional BCs (such as CC, CP, CF, FF, PP, and CP) may not cover all possible conditions at the ends of the model and therefore miss some natural frequencies.

In this article, by defining a linear and a torsional spring at each end of MWNT, and through changing their stiffness, the model covers all possible BCs for in-plane vibration of CNTs (Fig. 1). Thus, to see the effects of boundary stiffness on the natural frequency, a dimensionless boundary stiffness parameter p is introduced as follows

$$p \equiv \frac{K_{LL}}{K_{LR}} = \frac{K_{TL}}{K_{TR}} \tag{15}$$

As this parameter varies, the BCs of the model and the natural frequencies change; so, $\omega = \omega(p)$.

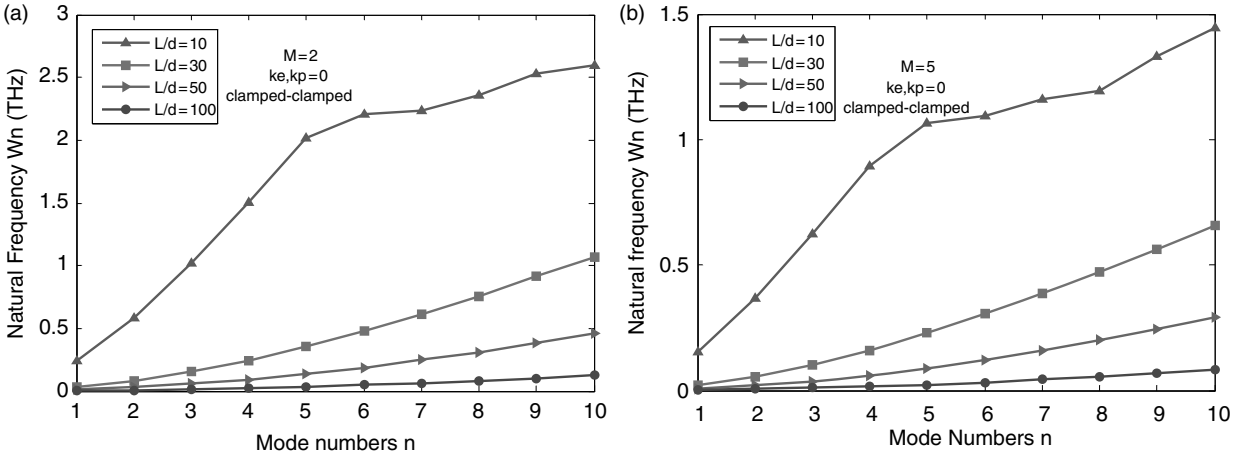

Fig. 2 Dimensional natural frequencies of a clamped–clamped MWNT against slenderness ratio L/d for: (a) $M=2$ and (b) $M=5$

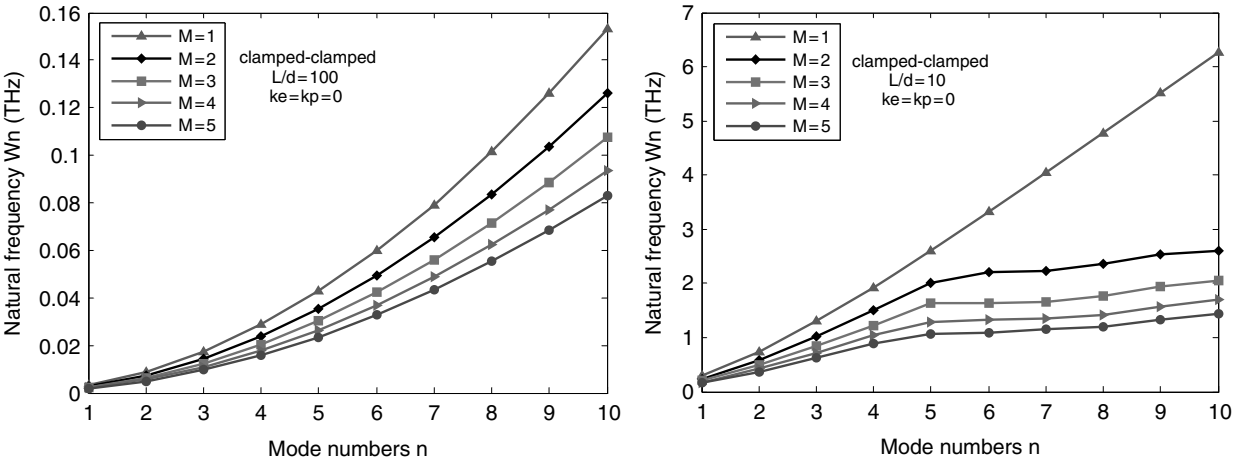

Fig. 3 Dimensional natural frequencies of a clamped–clamped MWNT with various numbers of walls for: (a) $L/d=10$ and (b) $L/d=100$

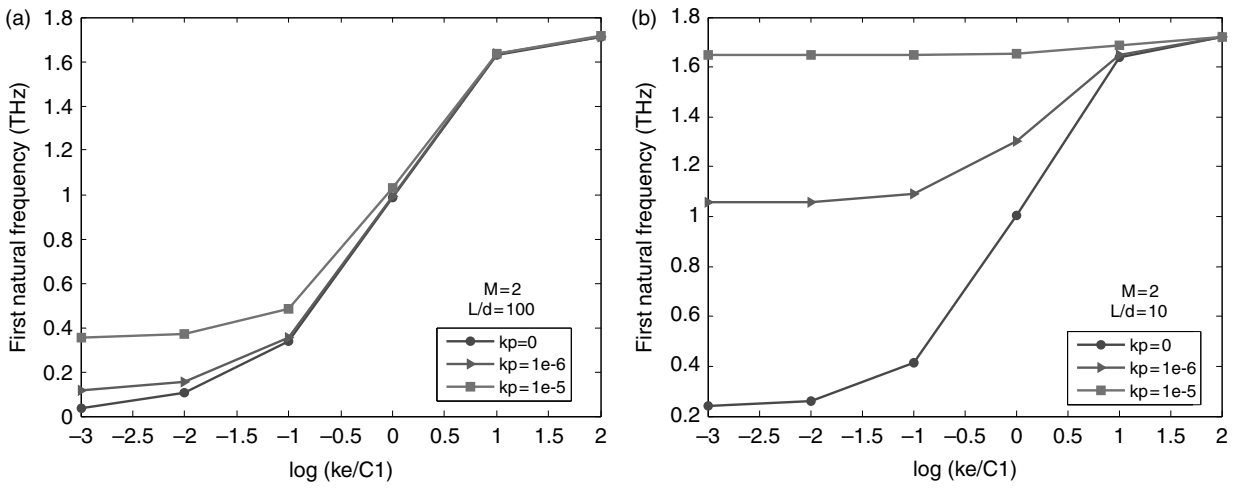

Fig. 4 The effects of the elastic constant k_e and shear constant k_p on the resonant frequencies of a MWNT

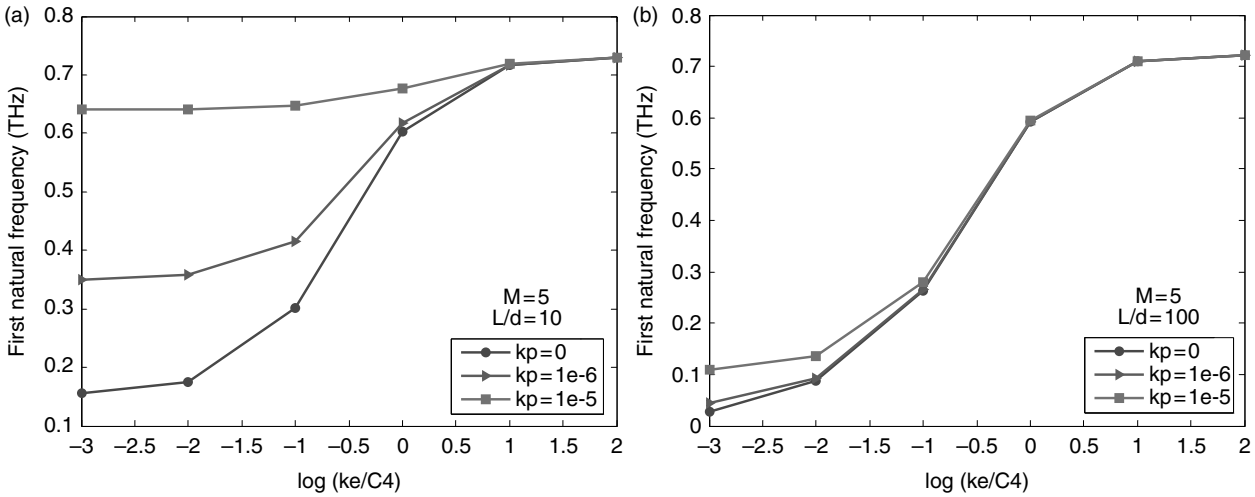

Fig. 5 The effects of the elastic constant k_e and shear constant k_p on the resonant frequencies of a MWNT

Table 5 Some numerical results to explain the effects of shear constant k_p of Pasternak model and aspect ratio L/d on the first natural frequency ω_1

	First natural frequency, ω_1 (THz)					
$K_e/C_1 = 0.01$	$M=2$			$M=5$		
	K_p			K_p		
	0	1.00E − 06	1.00E − 05	0	1.00E − 06	1.00E − 05
$L/d=10$	0.269	1.059 1	1.648 9	0.162 3	0.352 4	0.641
$L/d=100$	0.107 6	0.156 2	0.370 4	0.052 7	0.062 4	0.116 9

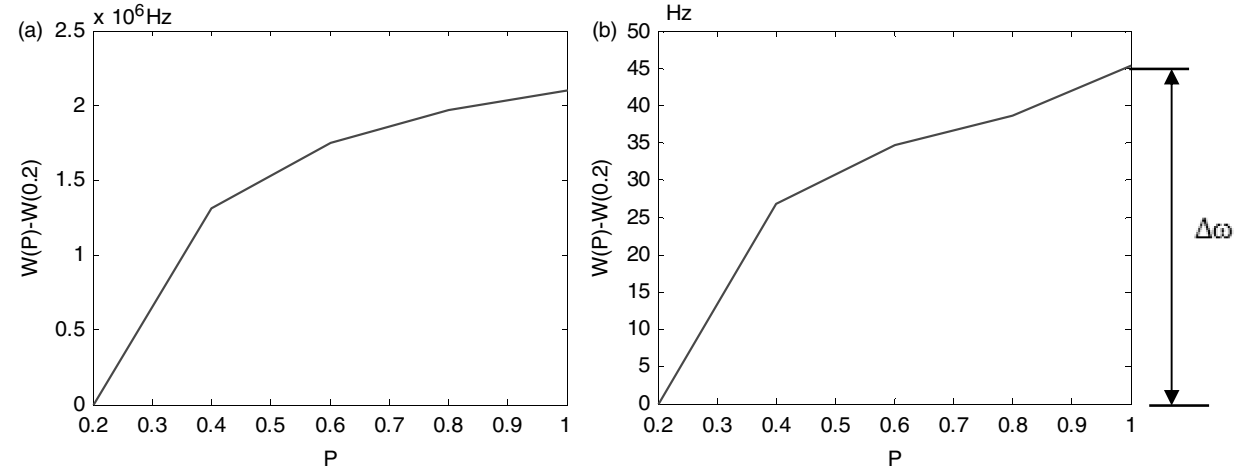

Fig. 6 The natural frequency as a function of dimensionless stiffness parameter p for a DWNT with: (a) $L/d=10$ and (b) $L/d=100$

In particular, for the sake of comparison, the natural frequency variation $\Delta\omega$ is also defined as

$$\Delta\omega \equiv \omega(1) - \omega(0.2) \tag{16}$$

Figure 6 reveal that the natural frequency of a DWNT increases with parameter p and frequency increases are more evident for models with $L/d=10$. For instance, the natural frequency variation $\Delta\omega$ for long CNT with $L/d=100$ is $\Delta\omega \cong 45$ Hz while for short CNT with $L/d=10$ is $\Delta\omega \cong 2.1$ MHz. This means that the effects of supports stiffness is more important for stubby nanotubes compared with long CNTs.

To analyse the effects of the parameter p on the changing natural frequency more clearly, the

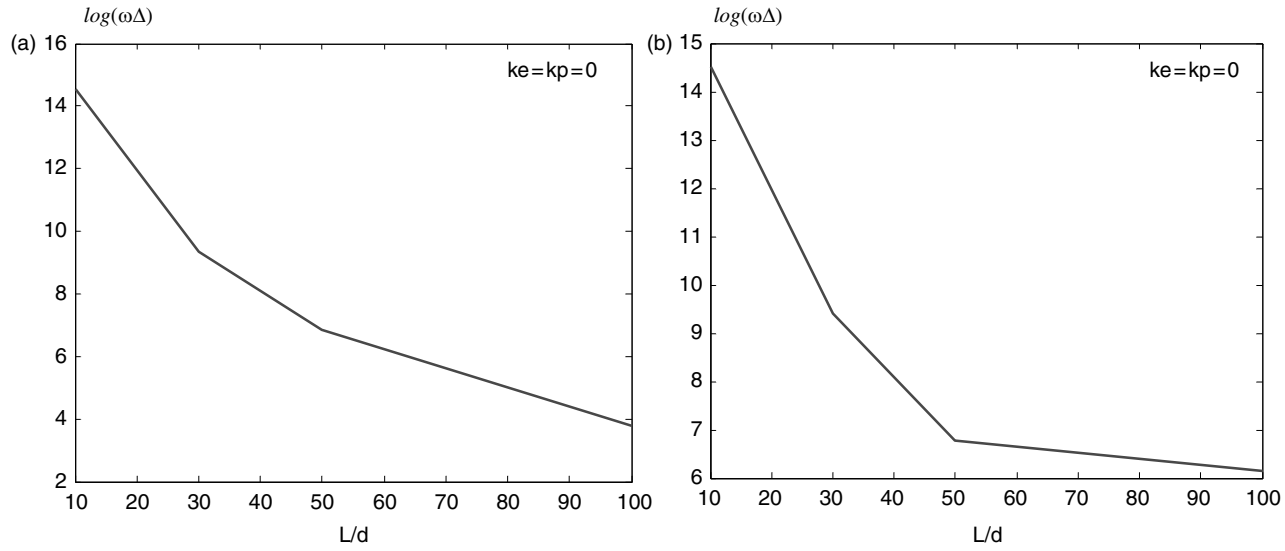

Fig. 7 The natural frequency variation L/d (a) for a DWNT $M=2$ and (b) for a MWNT $M=5$

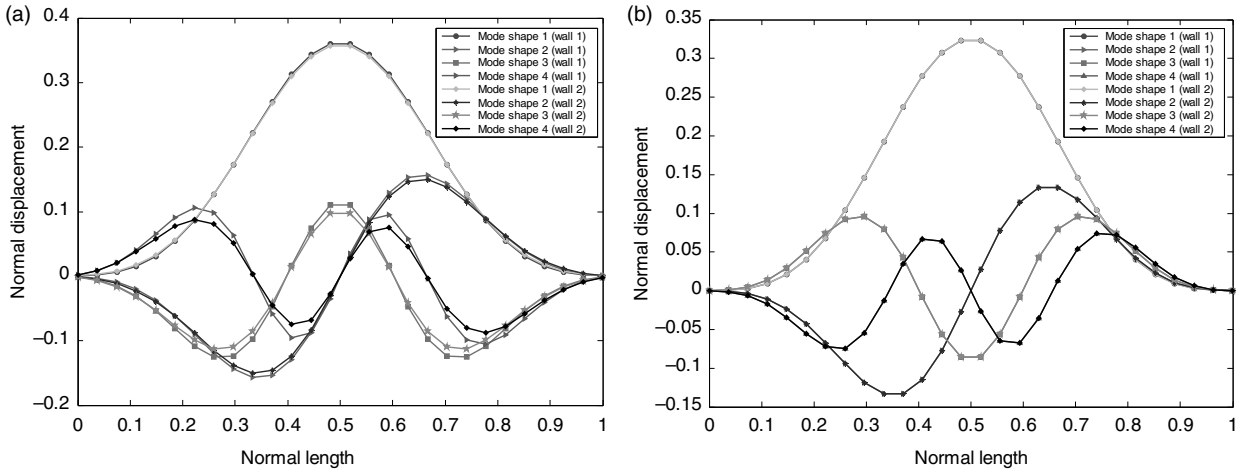

Fig. 8 The first four mode shapes for a DWNT ($M=2$) for two walls with: (a) $L/d=10$ and (b) $L/d=100$

natural frequency variation $\Delta\omega$ has been plotted with aspect ratio L/d for a DWNT ($M=2$) and a MWNT ($M=5$), as shown in Fig. 7. These figures demonstrate that the effect of boundary stiffness on the natural frequency is very important for short CNTs with small values of L/d. In other words, for vibrational models, an exact description of boundary conditions is not vital for long CNTs in comparison to stubby nanotubes. Moreover, evaluating Fig. 7(a) and (b) reveals that the stiffness of the ends of CNTs affects the natural frequency of MWNT ($M=5$) more significantly in comparison with DWNT ($M=2$). This means that increasing the number of walls causes BCs to become a more effective parameter for the natural frequencies of a nanotube.

7.3 Mode shapes

The present vibrational model is a general model, which can account for the mode shapes of a MWNT regardless of the number of the walls and the BCs. For instance, the first four mode shapes of a DWNT ($M=2$) have been drawn in Fig. 8 for the two walls with two different aspect ratios. Meanwhile, to see the effects of the number of walls M on the mode shapes, Fig. 9 shows the similar mode shapes for a MWNT ($M=5$). It is found from the figures that the difference between corresponding mode shapes of wall one and wall two tend towards each other with increasing the aspect ratio L/d of the CNT. In fact, for long slender CNTs, the relative internal vibrations of walls diminish and all walls vibrate in the same manner

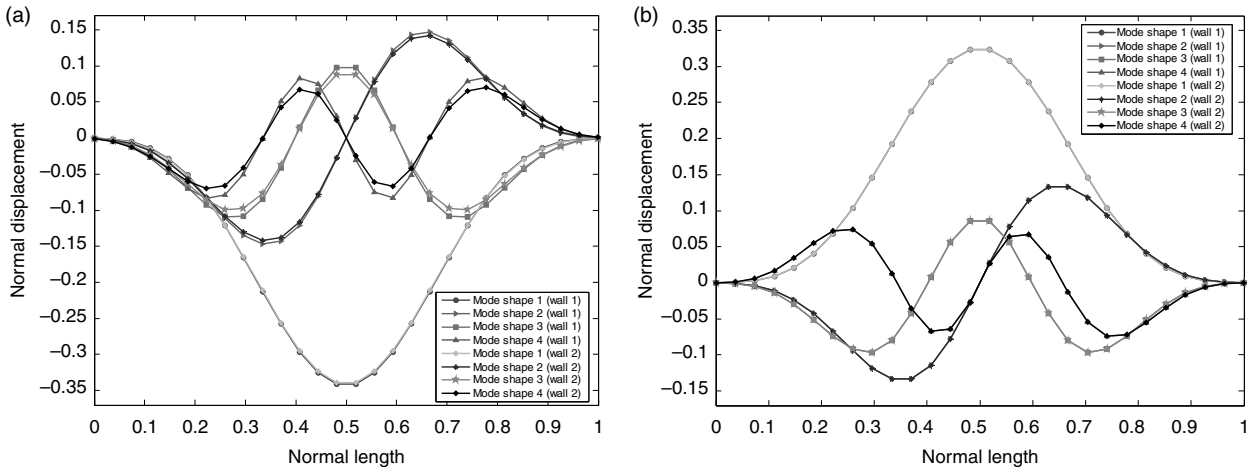

Fig. 9 First four mode shapes for a MWNT ($M=5$) for two inner walls with: (a) $L/d=10$ and (b) $L/d=100$

approximately. In addition, comparison of Figs 8 and 9 for $L/d=10$ or $L/d=100$ indicates that the number of walls M does not markedly affect the corresponding mode shapes.

8 CONCLUSIONS

In this study, for the first time, GDQM has been applied to solve a general vibrational model of MWNTs based on the Timoshenko elastic beam theory. The model covers all possible BCs, and the Pasternak-type foundation model, and it has no limitation dependent on the number of walls. Moreover, the non-coaxial vibration of MWNTs is taken into account using vdW interwall forces. The obtained results, which are in good agreement with previous simpler models, show that the natural frequencies of CNTs are sensitive to the stiffness of the medium, number of walls, and aspect ratio. The natural frequencies increase with elastic and shear constants of the Pasternak medium while, with increasing number of walls and aspect ratio, the natural frequencies decrease. Applying torsional and linear stiffnesses in each end of MWNT has made this model closer to real conditions, especially in nanocomposites. The results indicate that the boundary stiffness of the nanotube plays a more important role in the natural frequencies of short nanotubes.

REFERENCES

1 **Iijima, S.** Helical microtubules of graphitic carbon. *Nature*, 1991, **354**(6348), 56–58.

2 **Chang, T.** and **Gao, H.** Size-dependent elastic properties of a single-walled carbon nanotube via a molecular mechanics model. *J. Mech. Phys. Solids*, 2003, **51**(6), 1059–1074.

3 **Wang, X., Wang, X. Y.,** and **Xiao, J.** A non-linear analysis of the bending modulus of carbon nanotubes with rippling deformations. *Compos. Struct.*, 2005, **69**(3), 315–321.

4 **Bernholc, J., Brabec, C., Buongiorno Nardelli, M., Maiti, A., Roland, C.,** and **Yakobson, B. I.** Theory of growth and mechanical properties of nanotubes. *Appl. Phys. A*, 1998, **67**(1), 39–46.

5 **Treacy, M. M. J., Ebbesen, T. W.,** and **Gibson, J. M.** Exceptionally high Young's modulus observed for individual carbon nanotubes. *Nature*, 1996, **381**(6584), 678–680.

6 **Wang, X.** Effective bending modulus of carbon nanotubes with rippling deformation. *Int. J. Solids Struct.*, 2004, **41**(22–23), 6429–6439.

7 **Wang, X. Y.** and **Wang, X.** Numerical simulation for bending modulus of carbon nanotubes and some explanations for experiment. *Composites Part B*, 2004, **35**(2), 79–86.

8 **Lau, A. K.-T.** and **Hui, D.** The revolutionary creation of new advanced materials–carbon nanotube composites. *Composites Part B*, 2002, **33**(4), 263–277.

9 **Dai, H., Hafner, J. H., Rinzler, A. G., Colbert, D. T.,** and **Smalley, R. E.** Nanotubes as nanoprobes in scanning probe microscopy. *Nature*, 1996, **384**(6605), 147–150.

10 **Yang, W., Wang, H. T.,** and **Hong, W.** The advancement of nanomechanics (continued). *Adv. Mech.*, 2003, **33**, 175–185.

11 **Chang, W.-J.** and **Lee, H.-L.** Free vibration of a single-walled carbon nanotube containing a fluid flow using the Timoshenko beam model. *Phys. Lett. A*, 2009, **373**(10), 982–985.

12 **Hsu, J.-C., Chang, R.-P.,** and **Chang, W.-J.** Resonance frequency of chiral single-walled carbon nanotubes using Timoshenko beam theory. *Phys. Lett. A*, 2008, **372**(16), 2757–2759.

13 **Wang, C. Y.** and **Zhang, L. C.** An elastic shell model for characterizing single-walled carbon nanotubes. *Nanotechnology*, 2008, **19**(19), 195704.

14 **Yoon, J., Ru, C. Q.,** and **Mioduchowski, A.** Vibration of an embedded multiwall carbon nanotube. *Compos. Sci. Technol.*, 2003, **63**(11), 1533–1542.

15 **Wang, X.** and **Cai, H.** Effects of initial stress on non-coaxial resonance of multi-wall carbon nanotubes. *Acta Mater.*, 2006, **54**(8), 2067–2074.

16 **Yoon, J., Ru, C. Q.,** and **Mioduchowski, A.** Sound wave propagation in multiwall carbon nanotubes. *J. Appl. Phys.*, 2003, **93**(8), 4801–4806.

17 **Yoon, J., Ru, C. Q.,** and **Mioduchowski, A.** Timoshenko-beam effects on transverse wave propagation in carbon nanotubes. *Composites Part B*, 2004, **35**(2), 87–93.

18 **Yoon, J., Ru, C. Q.,** and **Mioduchowski, A.** Terahertz vibration of short carbon nanotubes modeled as Timoshenko beams. *J. Appl. Mech.*, 2005, **72**, 10–17.

19 **Wang, C. M., Tan, V. B. C.,** and **Zhang, Y. Y.** Timoshenko beam model for vibration analysis of multi-walled carbon nanotubes. *J. Sound Vib.*, 2006, **294**(4–5), 1060–1072.

20 **He, X. Q., Eisenberger, M.,** and **Liew, K. M.** The effect of van der Waals interaction modeling on the vibration characteristics of multiwalled carbon nanotubes. *J. Appl. Phys.*, 2006, **100**(12), 124317.

21 **Xu, K. Y., Guo, X. N.,** and **Ru, C. Q.** Vibration of a double-walled carbon nanotube aroused by nonlinear intertube van der Waals forces. *J. Appl. Phys.*, 2006, **99**(6), 064303–064307.

22 **Ru, C. Q.** Column buckling of multiwalled carbon nanotubes with interlayer radial displacements. *Phys. Rev. B*, 2000, **62**(24), 16962.

23 **Zhang, Y. Y., Wang, C. M.,** and **Tan, V. B. C.** Buckling of multiwalled carbon nanotubes using Timoshenko beam theory. *J. Eng. Mech.*, 2006, **132**(9), 952–958.

24 **Ruge, P.** and **Birk, C.** A comparison of infinite Timoshenko and Euler-Bernoulli beam models on Winkler foundation in the frequency- and time-domain. *J. Sound Vib.*, 2007, **304**(3–5), 932–947.

25 **Zhang, Y. Q., Lu, Y.,** and **Ma, G. W.** Effect of compressive axial load on forced transverse vibrations of a double-beam system. *Int. J. Mech. Sci.*, 2008, **50**(2), 299–305.

26 **Liew, K. M., He, X. Q.,** and **Kitipornchai, S.** Buckling characteristics of embedded multi-walled carbon nanotubes. *Proc. R. Soc. A*, 2005, **461**(2064), 3785–3805.

27 **Kitipornchai, S., He, X. Q.,** and **Liew, K. M.** Buckling analysis of triple-walled carbon nanotubes embedded in an elastic matrix. *J. Appl. Phys.*, 2005, **97**(11), 1–7.

28 **Murmu, T.** and **Pradhan, S. C.** Buckling analysis of a single-walled carbon nanotube embedded in an elastic medium based on nonlocal elasticity and Timoshenko beam theory and using DQM. *Physica E*, 2009, **41**(7), 1232–1239.

29 **Demir, C., Civalek, O.,** and **Akgöz, B.** Free vibration analysis of carbon nanotubes based on shear deformable beam theory by Discrete singular convolution technique. *Math. Comput. Appl.*, 2010, **15**(1), 57–65.

30 **Pradhan, S. C.** and **Murmu, T.** Small-scale effect on vibration analysis of single-walled carbon nanotubes embedded in an elastic medium using nonlocal elasticity theory. *J. Appl. Phys.*, 2009, **105**(12), 124306.

31 **Tong, F. M., Wang, B.,** and **Adhikari, S.** Axial buckling of multiwall carbon nanotubes with heterogeneous boundaries. *J. Appl. Phys.*, 2009, **105**(9), 094325.

32 **Chowdhury, R., Wang, C. Y.,** and **Adhikari, S.** Low frequency vibration of multiwall carbon nanotubes with heterogeneous boundaries. *J. Phys. D: Appl. Phys.*, 2010, **43**(8), 085405.

33 **Wu, T. Y., Liu, G. R.,** and **Wang, Y. Y.** Application of the generalized differential quadrature rule to initial–boundary–value problems. *J. Sound Vib.*, 2003, **264**(4), 883–891.

34 **Wu, T. Y.** and **Liu, G. R.** Generalized differential quadrature rule for initial-value differential equations. *J. Sound Vib.*, 2000, **233**(2), 195–213.

35 **Wu, T. Y.** and **Liu, G. R.** Free vibration analysis of circular plates with variable thickness by the generalized differential quadrature rule. *Int. J. Solids Struct.*, 2001, **38**(44–45), 7967–7980.

36 **Wu, T. Y., Wang, Y. Y.,** and **Liu, G. R.** A generalized differential quadrature rule for bending analysis of cylindrical barrel shells. *Comput. Meth. Appl. Mech. Eng.*, 2003, **192**(13–14), 1629–1647.

37 **Liu, G. R.** and **Wu, T. Y.** In-plane vibration analyses of circular arches by the generalized differential quadrature rule. *Int. J. Mech. Sci.*, 2001, **43**(11), 2597–2611.

38 **Hong, C. C., Liao, H. W., Lee, L. T., Ke, J. B.,** and **Jane, K. C.** Thermally induced vibration of a thermal sleeve with the GDQ method. *Int. J. Mech. Sci.*, 2005, **47**(12), 1789–1806.

39 **Lin, W.** and **Qiao, N.** In-plane vibration analyses of curved pipes conveying fluid using the generalized differential quadrature rule. *Comput. Struct.*, 2008, **86**(1–2), 133–139.

40 **Wang, L., Ni, Q., Li, M.,** and **Qian, Q.** The thermal effect on vibration and instability of carbon nanotubes conveying fluid. *Physica E*, 2008, **40**(10), 3179–3182.

41 **Aydogdu, M.** Vibration of multi-walled carbon nanotubes by generalized shear deformation theory. *Int. J. Mech. Sci.*, 2008, **50**(4), 837–844.

42 **Tornabene, F.** and **Viola, E.** Vibration analysis of spherical structural elements using the GDQ method. *Comput. Math. Appl.*, 2007, **53**(10), 1538–1560.

43 **Viola, E., Dilena, M.,** and **Tornabene, F.** Analytical and numerical results for vibration analysis of multi-stepped and multi-damaged circular arches. *J. Sound Vib.*, 2007, **299**(–2), 143–163.

44 **Tornabene, F.** and **Viola, E.** 2-D solution for free vibrations of parabolic shells using generalized differential quadrature method. *Eur. J. Mech. A Solids*, 2008, **27**(6), 1001–1025.

APPENDIX

Notation

A	cross-sectional area
c_j	vdW interaction coefficients
E	Young's modulus
G	shear modulus
k_e	elastic Winkler foundation coefficients
k_p	shear stiffnesses of the foundation
I	second moment of area of cross-section
K	shear correction factor
K_{LL}	linear stiffness for left end of CNT
K_{LR}	linear stiffness for right end of CNT
K_{TR}	torsional stiffness for left end of CNT
K_{TR}	torsional stiffness for right end of CNT
M	number of walls
P	pressure per unit axial length
R_j	average radius of jth tube
t	effective thickness of single-walled nanotubes
t'	distance of between two adjacent nanotubes
w	transverse deflection
x	axial coordinate
ρ	mass density per unit volume
ν	Poisson's ratio
φ	slope of beam